Optimal control of coupled quantum systems based on the first-order Magnus expansion: Application to multiple dipole-dipole-coupled molecular rotors

Andrew Ma [1,*] Alicia B. Magann [2,†] Tak-San Ho [3,‡] and Herschel Rabitz [3,§]

[1]*Department of Physics, Princeton University, Princeton, New Jersey 08544, USA*

[2]*Department of Chemical and Biological Engineering, Princeton University, Princeton, New Jersey 08544, USA*

[3]*Department of Chemistry, Princeton University, Princeton, New Jersey 08544, USA*

(Received 17 February 2020; accepted 17 June 2020; published 30 July 2020)

This paper presents a method for performing approximate optimal control simulations for quantum systems with multiple coupled degrees of freedom. The time evolution is simulated using the first-order Magnus expansion in the interaction picture, where the couplings between different degrees of freedom are treated as the perturbation. A numerical implementation procedure is presented that leverages upon pairwise couplings and the separability of the zeroth-order time evolution operator to achieve a reduced computational cost, which is analyzed with respect to the number of degrees of freedom. The formulation is compatible with gradient-free methods to optimize the control field, and a stochastic hill climbing algorithm is adopted for this purpose. As illustrations, optimal control simulations are performed for systems of two and three dipole-dipole-coupled molecular rotors under the influence of a control field. For the two-rotor system, the field is optimized to achieve either orientation or entanglement objectives. For the three-rotor system, the field is optimized either to orient all three rotors in the same direction or to orient one rotor in a particular direction while the other two rotors point in the opposite direction.

DOI: 10.1103/PhysRevA.102.013115

I. INTRODUCTION

There is considerable interest in using optimally shaped fields to control the dynamics of quantum systems [1–5]. Such fields can be found using iterative optimization methods, such as gradient [6–9] or gradient-free [10–12] procedures. Applications lie in a wide range of areas, including quantum information science [13–15], chemical reactions [16], nanostructured materials [17], and high-harmonic generation [18].

Optimal control simulations for quantum systems with multiple coupled degrees of freedom are particularly challenging, since the dimensionality of the Hilbert space scales exponentially with the number of degrees of freedom [1,19,20]. To address this issue, various approximations have been employed, including semiclassical Gaussian wave packets [21,22], time-dependent Hartree (TDH) [12,23,24], multiconfigurational time-dependent Hartree (MCTDH) [25–27], and the time-dependent density matrix renormalization group (tDMRG) [20].

This paper takes an alternative approach by considering the Magnus expansion to approximate the time evolution operator. A common implementation of the Magnus expansion rests on splitting the Hamiltonian into an unperturbed term and a perturbative term, and then utilizing the interaction picture [28]. The first-order Magnus expansion has been applied to a variety of problems [28], including molecular alignment and orientation in ultrafast laser fields [29] and molecular collisions in the sudden regime [30].

This paper adopts the first-order Magnus expansion for quantum optimal control of systems with multiple coupled degrees of freedom. Specifically, the couplings between degrees of freedom are treated as the perturbation and the expansion is evaluated only once at the final time T. This approach can be readily combined with gradient-free methods, and the present work uses a stochastic hill climbing algorithm [12,31]. The method performs best for systems with weakly coupled degrees of freedom. Overall, there are three primary benefits to the method: (1) It is not restricted to the weak control field regime since the control field lies in the zeroth-order portion of the Hamiltonian, (2) there is no need for expensive gradient computations or the evaluation of the system state at intermediate time steps, and (3) common pairwise couplings allow for an accelerated implementation. As such, there are benefits both for the scope of utility [feature (1)] and for the computational cost [features (2) and (3)]. The computational scaling of the method is analyzed with respect to the number of degrees of freedom N. The technique is illustrated numerically, including a characterization of its accuracy, for optimal control of two and three dipole-dipole-coupled molecular rotors. The control objectives for these illustrations include (i) orientation of all rotors in the same direction, (ii) orientation of rotors in opposing directions, and (iii) entanglement between rotors.

*Present address: Department of Electrical Engineering and Computer Science, Massachusetts Institute of Technology, Cambridge, Massachusetts 02139, USA; andrewm1@mit.edu

†amagann@princeton.edu

‡tsho@princeton.edu

§hrabitz@princeton.edu

Previously, quantum control of rotor systems has been studied using numerically exact simulations for one-rotor [32–35] and two-rotor [36–38] cases, as well as in the TDH approximation for systems of up to five rotors [12]. Additionally, single rotors were used in the study of the nonlinear local control method [39]. In the context of phase transitions, lattices of rotors have been treated using the path integral ground state (PIGS) quantum Monte Carlo method [40]. Systems of three rotors have also been used to study the influence of intrinsic decoherence [41].

The remainder of the paper is organized as follows. Section II provides relevant theoretical background. Section III presents the method for approximate quantum optimal control based on the first-order Magnus expansion, including both the mathematical formulation and the numerical implementation procedure for the approximate time evolution, as well as a description of the optimization algorithm. Section IV presents an analysis of the computational cost and scaling of the method. Section V gives a theoretical description of the model rotor systems and control objectives. Section VI gives benchmark simulations showing the effect of rotor separation on the quality of the approximate time evolution. Section VII presents approximate optimal control simulation results for the rotor systems. Finally, Sec. VIII provides conclusions and a discussion of possible future work. Extensive Supplemental Material is online [42], which is referenced throughout the paper to provide further details.

II. THEORETICAL BACKGROUND

A. Quantum optimal control theory

Quantum optimal control theory generally seeks to identify a time-dependent control field $\varepsilon(t)$, $t \in [0, T]$, that maximizes a given objective functional $J[T, \varepsilon(\cdot)]$ at the final time T [1,3,5]. Besides the control objective, $J[T, \varepsilon(\cdot)]$ may depend as well on features that favor certain field characteristics [1]. In the remainder of the paper, the objective functional is chosen to be the expectation value of an observable O, i.e.,

$$\max_{\varepsilon(\cdot)} J[T] = \max_{\varepsilon(\cdot)} \langle O \rangle(T), \tag{1}$$

where $\langle O \rangle(t) \equiv \langle \Psi(t)|O|\Psi(t)\rangle$, with $|\Psi(t)\rangle$ being the solution to the time-dependent Schrödinger equation,

$$i\hbar \frac{\partial}{\partial t}|\Psi(t)\rangle = H(t)|\Psi(t)\rangle, \tag{2}$$

at time t given the initial state $|\Psi(0)\rangle$.

The exact solution $|\Psi(t)\rangle$ to Eq. (2) is given by

$$|\Psi(t)\rangle = U(t)|\Psi(0)\rangle, \tag{3}$$

with $U(t) \equiv U(t, 0)$ being the time evolution operator from 0 to t,

$$U(t) = \mathcal{T}\left(\exp\left(-\frac{i}{\hbar}\int_0^t H(t')dt'\right)\right), \tag{4}$$

where $\mathcal{T}$ is the time ordering operator. In practice, the time interval $[0, T]$ is often discretized into n equally spaced, sufficiently small time steps $\Delta t \equiv \frac{T}{n}$, so that Eq. (3) can be numerically solved as

$$|\Psi(T)\rangle = \left(\prod_{k=1}^{n} U(k\Delta t, (k-1)\Delta t)\right)|\Psi(0)\rangle, \tag{5}$$

where $U(k\Delta t, (k-1)\Delta t) \equiv \exp(-\frac{i}{\hbar}H(k\Delta t)\Delta t)$, and the product is assumed to be time ordered. The expression in Eq. (5) converges to the exact solution in Eq. (4) for $n \to \infty$. This paper will refer to Eq. (5) with sufficiently large n as the exact simulation (see [43] for discussion of time step size). The numerical implementation of Eq. (5) requires the exponentiation of the matrix $(-\frac{i}{\hbar}H(k\Delta t)\Delta t)$ at every time step [44], which can be computationally prohibitive for systems with many coupled degrees of freedom.

B. Magnus expansion in the interaction picture

This subsection reviews the Magnus expansion in the interaction picture for solving Eq. (2) (e.g., see [28] for more details). This expansion will be applied to optimal control of coupled quantum systems in Sec. III A.

The Hamiltonian $H(t)$ is decomposed into an unperturbed term $H^{(0)}(t)$ and a perturbation term $H^{(1)}(t)$,

$$H(t) = H^{(0)}(t) + H^{(1)}(t). \tag{6}$$

Commonly $H^{(0)}$ is taken as time independent, but in the context of the applications considered here it will be advantageous to consider $H^{(0)} = H^{(0)}(t)$ to include the time-dependent control field (this will be discussed in Sec. III). The time evolution operator $U(t)$ defined in Eq. (4) is then factored into the product

$$U(t) = U^{(0)}(t)U_I(t), \tag{7}$$

where

$$U^{(0)}(t) \equiv \mathcal{T}\left(\exp\left(-\frac{i}{\hbar}\int_0^t H^{(0)}(t')dt'\right)\right), \tag{8}$$

and

$$U_I(t) \equiv \mathcal{T}\left(\exp\left(-\frac{i}{\hbar}\int_0^t H_I^{(1)}(t')dt'\right)\right) \tag{9}$$

is the interaction picture time evolution operator with

$$H_I^{(1)}(t) \equiv U^{(0)}(t)^\dagger H^{(1)}(t)U^{(0)}(t). \tag{10}$$

The full Magnus expansion for $U_I(t)$ is

$$U_I(t) = \exp(\Omega_I(t)), \tag{11}$$

where

$$\Omega_I(t) \equiv \sum_{k=1}^{\infty} \Omega_{I,k}(t), \tag{12}$$

with $\Omega_{I,k}(t)$ being the kth-order term. The kth-order Magnus expansion is given by truncating the series in Eq. (12) after the term $\Omega_{I,k}(t)$ [the zeroth-order approximation is just $U(t) \approx U^{(0)}(t)$]. Truncations to any order preserve unitarity of $U(t)$, which guarantees conservation of total probability.

In particular, the first-order term in Eq. (12) is

$$\Omega_{I,1}(t) = -\frac{i}{\hbar}\int_0^t H_I^{(1)}(t')dt', \tag{13}$$

and the approximate time evolution operator in the first-order Magnus expansion is

$$U_{M1}(t) = U^{(0)}(t)\exp(\Omega_{I,1}(t)). \tag{14}$$

Substituting $U_{M1}(t)$ in Eq. (14) for $U(t)$ in Eq. (3) and evaluating at $t = T$ yields the approximate final state,

$$|\Psi_{M1}(T)\rangle = U^{(0)}(T)\exp(\Omega_{I,1}(T))|\Psi(0)\rangle. \tag{15}$$

Note that in this notation, U_{M1} and $|\Psi_{M1}\rangle$ correspond to the entire first-order Magnus expansion, and not just the correction to the zeroth-order term. Importantly, Eq. (15) directly obtains the final state from the initial state, without the need for computing intermediate states. This feature would also apply to the truncation of the Magus expansion at any order.

III. GENERAL METHODOLOGY

This section presents a general approach for optimal control simulations of quantum systems with multiple coupled degrees of freedom using the first-order Magnus expansion. Its accuracy should be best for systems with weak couplings W and an adequately short fixed propagation time T. Section III A describes the mathematical formulation of the approximation of the time evolution. Section III B presents the numerical implementation of this formulation. Section III C describes combining the approximate time evolution with gradient-free algorithms for control field optimization.

A. First-order Magnus expansion for weakly coupled quantum systems

This subsection applies the first-order Magnus expansion in the interaction picture, described in Sec. II B, to weakly coupled quantum systems under the influence of a control field. The restriction to weak couplings is consistent with the truncation of the Magnus expansion to first order.

The quantum system is assumed to be governed by a Hamiltonian of the form

$$H(q_1, q_2, \ldots, q_N, t) = \sum_{i=1}^{N}(T(q_i) + V_i(q_i, t)) + W(q_1, q_2, \ldots, q_N), \tag{16}$$

where N is the number of degrees of freedom, q_i is the coordinate for the ith degree of freedom, $T_i(q_i)$ is the associated kinetic energy term, $V_i(q_i, t)$ is the local potential that depends only on the ith degree of freedom, and $W(q_1, q_2, \ldots, q_N)$ contains the couplings between different degrees of freedom (assumed to be time independent). The time dependence of each $V_i(q_i, t)$ term arises as a result of the control field $\varepsilon(t)$.

This paper uses the first-order Magnus expansion in the interaction picture [i.e., Eq. (15)] to approximate the time evolution corresponding to the Hamiltonian in Eq. (16). An issue of key importance is how to judiciously choose the unperturbed term $H^{(0)}$ and the perturbation $H^{(1)}$ in Eq. (6), since this choice strongly influences both the regime of utility of the approximation as well as its computational cost. The following formulation includes the control field $\varepsilon(t)$ in the zeroth-order Hamiltonian $H^{(0)}$, which contrasts with the more standard choice of treating the field as entering into the perturbation [29,45]. Specifically, the Hamiltonian [Eq. (16)] is decomposed into the perturbation term containing the couplings,

$$H^{(1)}(q_1, q_2, \ldots, q_N) = W(q_1, q_2, \ldots, q_N), \tag{17}$$

and the unperturbed term,

$$H^{(0)}(q_1, q_2, \ldots, q_N, t) = \sum_{i=1}^{N} H_i(q_i, t), \tag{18}$$

where

$$H_i(q_i, t) \equiv T_i(q_i) + V_i(q_i, t) \tag{19}$$

is the coupling-free Hamiltonian for the ith degree of freedom.

In this particular scenario the zeroth-order time evolution operator $U^{(0)}(q_1, q_2, \ldots, q_N, t)$ [cf. Eq. (8)] is fully separable as

$$U^{(0)}(q_1, q_2, \ldots, t) = \bigotimes_{i=1}^{N} U_i(q_i, t), \tag{20}$$

where $\bigotimes$ denotes a tensor product and

$$U_i(q_i, t) \equiv \mathcal{T}\left(\exp\left(-\frac{i}{\hbar}\int_0^t H_i(q_i, t')dt'\right)\right) \tag{21}$$

is the time evolution operator associated with $H_i(q_i, t)$. Consequently, substituting Eq. (20) into Eq. (15) produces the expression for the approximate final state under the first-order Magnus expansion,

$$|\Psi_{M1}(T)\rangle = \left(\bigotimes_{i=1}^{N} U_i(q_i, T)\right)\exp(\Omega_{I,1}(T))|\Psi(0)\rangle, \tag{22}$$

where

$$\Omega_{I,1}(T) = -\frac{i}{\hbar}\int_0^T dt'\left(\bigotimes_{i=1}^{N} U_i(q_i, t')^{\dagger}\right)W(q_1, q_2, \ldots, q_N) \times \left(\bigotimes_{i'=1}^{N} U_{i'}(q_{i'}, t')\right). \tag{23}$$

The expected advantages of the choice of $H^{(1)}$ and $H^{(0)}$ in Eqs. (17) and (18) are twofold: (1) good accuracy beyond the weak control field regime and (2) decreased computational cost compared to exact simulations. The former is realized due to the inclusion of the control field in $H^{(0)}$. Specifically, this inclusion makes the matrix norm of the perturbation term in the interaction picture ($||H_I^{(1)}(t)||$) independent of the control field [46]. The latter advantage will be discussed in Secs. III B and IV. The mathematical formulation can also be adapted to include the second-order term in the Magnus expansion or a multistep Magnus scheme, which are described in Secs. S1.1 and S1.2, respectively (the paper will denote S as the Supplemental Material) [42].

B. Numerical implementation

This subsection presents the procedure for numerically implementing the formulation described in Sec. III A. The procedure is first presented for arbitrary Hamiltonians with multiple degrees of freedom, followed by consideration of the

specific case of *pairwise* couplings. Implementation details as well as computational cost analysis are presented in Sec. S2 [42]. Although the simulations in this paper are restricted to the first-order approximation, a suggested numerical procedure and the associated computational cost analysis for the second-order approximation are presented in Sec. S3 as a look ahead [42]. In what follows, the coordinate arguments are suppressed for conciseness.

1. General implementation

A three-part procedure is presented below for numerically implementing the first-order Magnus expansion in Eq. (22). The time interval is uniformly discretized into n time steps of size $\Delta t = \frac{T}{n}$, which are sufficiently small to give reliable results [43].

Part I: $U_i(k\Delta t)$ is computed by Eq. (21), for $1 \leqslant i \leqslant N$ and $1 \leqslant k \leqslant n$, recursively starting with $U_i(0) = I$:

$$U_i(k\Delta t) = \exp\left(-\frac{i}{\hbar}H_i(k\Delta t)\Delta t\right)U_i((k-1)\Delta t). \tag{24}$$

Part II: $\Omega_{I,1}(T)$ is computed by numerically evaluating the integral in Eq. (23) using n-point rectangular quadrature, i.e.,

$$\Omega_{I,1}(T) = -\frac{i}{\hbar}\sum_{k=1}^{n}\Delta t\left(\bigotimes_{i=1}^{N}U_i(k\Delta t)^\dagger\right)W\left(\bigotimes_{i'=1}^{N}U_{i'}(k\Delta t)\right). \tag{25}$$

Part III: The final state $|\Psi_{M1}(T)\rangle$ at time $T = n\Delta t$ is computed with Eq. (22).

Importantly, this numerical scheme [i.e., by Eq. (22)] allows for computing the final state without explicitly computing the state $|\Psi(k\Delta t)\rangle$ or the time evolution operator $U(k\Delta t, (k-1)\Delta t)$ at each intermediate time step (i.e., the computations in Eq. (5) can be avoided).

2. Implementation for pairwise couplings

Many Hamiltonians contain only pairwise coupling terms. For such Hamiltonians, a numerical procedure for Sec. III B 1 *Part II* is described, which exploits separability to avoid computing matrix products in the full N-body Hilbert space. Specifically, Eq. (25) is evaluated for generic pairwise couplings of the form

$$W = \sum_{1\leqslant i<j\leqslant N} W_{ij}, \tag{26}$$

where W_{ij} couples the ith and jth degrees of freedom (e.g., see examples in Sec. V A). For simplicity, the Hilbert space of each individual degree of freedom i (denoted by $\mathcal{H}_i$) is considered to be of the same dimension D, so that the full N-body Hilbert space has dimension D^N; this restriction can easily be lifted.

The direct approach would be to simply form and then multiply together the $D^N \times D^N$ matrices $\bigotimes_{i=1}^{N}U_i(k\Delta t)^\dagger$, W and $\bigotimes_{i'=1}^{N}U_{i'}(k\Delta t)$ at each time step k, followed by summing over all time steps. When W assumes the pairwise form given in Eq. (26), then Eq. (25) can be rewritten as

$$\Omega_{I,1}(T) = \sum_{1\leqslant i<j\leqslant N}\gamma_{ij}, \tag{27}$$

where

$$\gamma_{ij} \equiv -\frac{i}{\hbar}\Delta t\sum_{k=1}^{n}\left(\bigotimes_{i'=1}^{N}U_{i'}(k\Delta t)^\dagger\right)W_{ij}\left(\bigotimes_{i''=1}^{N}U_{i''}(k\Delta t)\right), \tag{28}$$

which can be expressed as

$$\gamma_{ij} = -\frac{i}{\hbar}\Delta t\sum_{k=1}^{n}(U_i(k\Delta t)^\dagger \otimes U_j(k\Delta t)^\dagger)W_{ij} \times (U_i(k\Delta t)\otimes U_j(k\Delta t)), \tag{29}$$

indicating that each γ_{ij} acts only on the ith and jth degrees of freedom. Therefore, Eq. (29) can be evaluated for each (i, j) within the D^2-dimensional Hilbert space $\mathcal{H}_i \otimes \mathcal{H}_j$, before all of the γ_{ij} are summed to get $\Omega_{I,1}(T)$. The cost of this implementation of *Part II* scales polynomially with respect to N, as opposed to the direct implementation of *Part II*, which scales exponentially with respect to N (see Sec. S2.2 [42]).

C. Control field optimization

For optimal control simulations with the first-order Magnus expansion that realize computational savings from skipping the intermediate states, it is necessary to choose an optimization algorithm that does not require knowledge of D^N-dimensional state vectors or $D^N \times D^N$ time evolution operators at intermediate times. Employing a gradient-free algorithm is a suitable approach for this purpose. All of the simulations in the paper adopt a stochastic hill climbing algorithm [12,31], which iteratively optimizes the control field $\varepsilon(t)$ starting from an initial trial field $\varepsilon_{\text{trial}}(t)$. At each iteration, a set of small random changes $\delta\varepsilon(t) \equiv \{\delta\varepsilon(t_k)\}$ are introduced, which are accepted only if they increase the value of the objective. The specific implementation is described in Sec. S4 [42].

IV. COMPUTATIONAL COST AND SCALING

This section analyzes the computational cost of a single iteration of the quantum control simulation. The analysis is restricted to the case of pairwise couplings [i.e., Eq. (26)]. We analyze only the cost of operations associated with simulating the time evolution from $t = 0$ to $t = T$. The amount of memory required and the overhead costs are not considered.

To estimate the computational cost and scaling with respect to D, n, and N, the analysis below considers the most expensive operations by counting the number of complex number multiplications [47]. The symbol O denotes an upper bound on the computational cost up to a multiplicative constant. When an explicit cost without the symbol O is given (e.g., $C_1 D^{\alpha N}$), it refers to the cost using currently known numerical methods.

The computational cost of each part of the numerical implementation presented in Sec. III B is analyzed in Sec. S2 [42]. In brief, the costs of *Part I*, *Part II*, and *Part III* are, respectively, $O(nND^3)$, $O(nN^2D^6)$, and $C_1D^{\alpha N} + 2D^{2N} + O(D^{N+1})$, where C_1 is a constant and $2 < \alpha \leqslant 3$. Therefore, the total computational cost of one full simulation of the time evolution becomes $C_1D^{\alpha N} + 2D^{2N} + O(D^{N+1}) + O(nN^2D^6)$.

The computational cost of the first-order Magnus expansion can be compared to that of the exact simulation in the large N limit. This comparison is only intended to give an estimate of the cost savings that may be possible, since both the approximate and exact simulations are computationally very intensive for truly large N. In this limit, the dominant costs of the first-order Magnus expansion and exact simulation are, respectively, $C_1 D^{\alpha N}$ and $C_1 n D^{\alpha N}$ (see Sec. S2.4 [42]). This result indicates an estimated $\frac{1}{n}$ improvement in computational cost, which is significant since the number of time steps n is generally large [43] (e.g., $n \sim 10^3$ to 10^4 for the numerical simulations in Sec. VII). The computational enhancement arises from sidestepping the need to determine the system state at intermediate time steps, together with the fact that the integral over all time steps can be evaluated in lower dimensional Hilbert spaces by exploiting the pairwise coupling form of W in Eq. (26). Note that we have not considered whether pairwise couplings can reduce the cost of the exact simulation (for more discussion, see Sec. S2.4 [42]).

In the analysis in Sec. S3, we show that in the large N limit the dominant computational cost of the second-order Magnus expansion should be the same as that of the first-order Magnus expansion (i.e., $C_1 D^{\alpha N}$) [42]. However, for practical applications (away from the large N limit) it is possible that the costs of the second-order and first-order Magnus expansions may be substantially different, since the upper bound shown for the cost of computing $\Omega_{I,2}(T)$ is significantly greater than the upper bound shown for computing $\Omega_{I,1}(T)$. As such, further analysis is needed to determine the utility of the second-order Magnus expansion for practical applications.

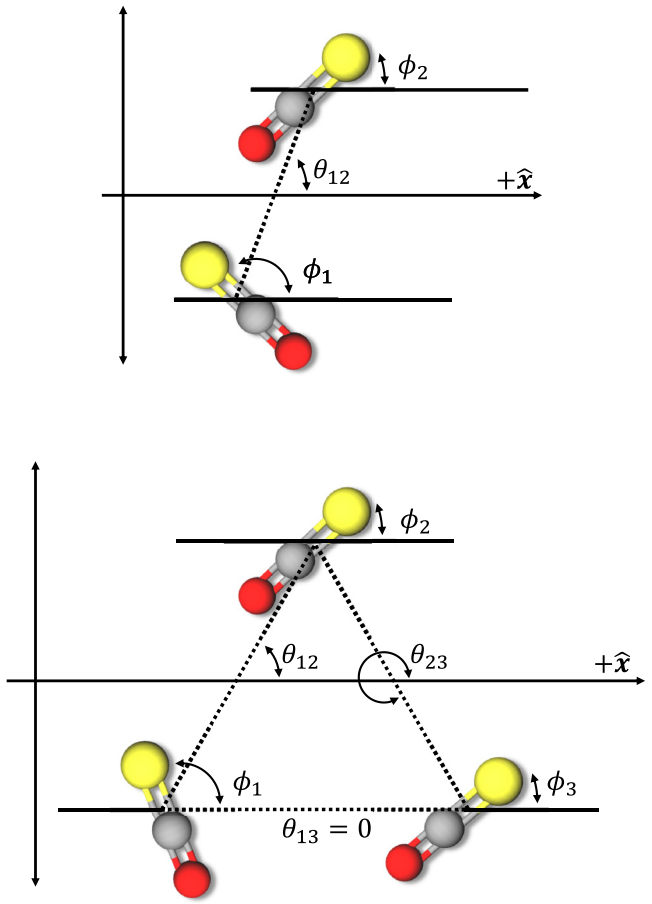

FIG. 1. (Top) Schematic of two coupled OCS molecules. The rotors are under the influence of a time-dependent control electric field $\varepsilon(t)$ polarized in the $\hat{\mathbf{x}}$ direction. ϕ_1 and ϕ_2 are the angles of rotor 1 and rotor 2 with respect to the polarization direction of the electric field. θ_{12} is the angle of the vector between the center of masses of rotors 1 and 2 with respect to the polarization direction of the electric field. (Bottom) Schematic of three coupled OCS molecules, using the analogous notation as in the two-rotor schematic. In both cases the rotors lie in a plane. The schematics are adapted from A. Magann *et al.* [12] with the permission of AIP Publishing.

V. DESCRIPTION OF THE ROTOR SYSTEM APPLICATIONS AND CORRESPONDING CONTROL OBJECTIVES

A. System description

1. General N-rotor system

The systems considered in the paper are multiple OCS molecules under the influence of a linearly polarized electric field. The molecules are modeled as rigid rotors in a planar configuration with dipole-dipole coupling between pairs of rotors. See [12] and [37] for a physical discussion of this circumstance. For a system of N such rotors, the Hamiltonian is given by

$$H(\phi_1, \ldots, \phi_N, t) = \sum_{i=1}^{N} \left(BL_i^2 - \mu\varepsilon(t)\cos\phi_i \right) + \sum_{1 \leqslant i < j \leqslant N} \frac{\mu^2}{4\pi\epsilon_0 R_{ij}^3} (\cos(\phi_i - \phi_j) - 3\cos(\phi_i - \theta_{ij})\cos(\phi_j - \theta_{ij})), \quad (30)$$

where $B \equiv \frac{\hbar^2}{2I} = 4.033 \times 10^{-24} J$ is the rotational constant [48], $L_i^2 = -\frac{\partial^2}{\partial\phi_i^2}$ is the squared angular momentum operator for the ith rotor, $\mu \equiv |\boldsymbol{\mu}_i| = 2.365 \times 10^{-30}$ C m [49] is the magnitude of the dipole moment of OCS, $\varepsilon(t)$ is the electric field amplitude at time t, ϕ_i is the angle between the ith rotor's dipole moment $\boldsymbol{\mu}_i$ and the electric field polarization (oriented in the $\hat{\mathbf{x}}$ direction), $\mathbf{R}_{ij}$ is the fixed relative position vector between the centers of mass of rotor i and rotor j, $R_{ij} \equiv |\mathbf{R}_{ij}|$ is its magnitude, and θ_{ij} is the fixed angle between $\mathbf{R}_{ij}$ and the electric field polarization. Labeled schematics for $N = 2$ and $N = 3$ are given in Fig. 1.

The couplings in the Hamiltonian in Eq. (30) are all pairwise, which permits utilizing the numerical technique for the first-order Magnus expansion described in Sec. III B 2. Specifically, $H_i(\phi_i, t) = BL_i^2 - \mu\varepsilon(t)\cos\phi_i$ for the coupling-free Hamiltonian of the ith rotor and $W_{ij} = \frac{\mu^2}{4\pi\epsilon_0 R_{ij}^3}(\cos(\phi_i - \phi_j) - 3\cos(\phi_i - \theta_{ij})\cos(\phi_j - \theta_{ij}))$ for the pairwise coupling between rotors i and j.

The simulations use the basis set given by $\{|m_1\rangle \otimes |m_2\rangle \cdots \otimes |m_N\rangle\}$, where $\{|m_i\rangle\}$ are the orthonormal eigenstates of the angular momentum operator L_i^2, satisfying $L_i^2|m_i\rangle = m_i^2|m_i\rangle$. The basis set is truncated to a sufficiently

large size for each application, such that m_i takes the values $-M, \ldots, -2, -1, 0, 1, 2, \ldots, M$ (consequently $D{=}2M{+}1$).

2. Two-rotor geometry and initial state

For all two-rotor simulations (in Secs. VI and VII), the geometry was $\theta_{12} = \frac{\pi}{2}$ and the initial state was $|\Psi(0)\rangle = |0\rangle \otimes |0\rangle$ [37]. Note that the rotors are identical in this system; in particular, $\langle \cos\phi_1 \rangle(t) = \langle \cos\phi_2 \rangle(t)$ at all times t, which is relevant for understanding the two-rotor orientation objective.

3. Three-rotor geometry and initial state

All three-rotor simulations (in Secs. VI and VII) are carried out in an equilateral triangle geometry with $\theta_{12} = \frac{\pi}{3}$, $\theta_{13} = 0$, $\theta_{23} = \frac{5\pi}{3}$, and $R_{12} = R_{13} = R_{23} \equiv R$, with an initial state given by $|\Psi(0)\rangle = |0\rangle \otimes |0\rangle \otimes |0\rangle$ [12]. Section S5 proves that for this three-rotor geometry and initial state, the following relationship holds at all times t [42]:

$$\langle \cos\phi_1 \rangle(t) = \langle \cos\phi_3 \rangle(t), \tag{31}$$

which is relevant for defining and understanding the control objectives. For completeness, Sec. S5 also proves the relationships $\langle \sin\phi_1 \rangle(t) = -\langle \sin\phi_3 \rangle(t)$ and $\langle \sin\phi_2 \rangle(t) = 0$ for this system [42].

B. Control objectives

1. Two-rotor objectives

For the two-rotor system described in Sec. V A 2, the following two objectives are considered.

(i) Orientation of the two rotors, where the objective functional is

$$J_{or}^{[2]}(T) \equiv \langle \cos\phi_1 + \cos\phi_2 \rangle(T), \tag{32}$$

which seeks to orient the rotors in the $+\hat{\mathbf{x}}$ direction.

(ii) Entanglement of the two rotors, where the objective functional is

$$J_{\text{ent}}^{[2]}(T) \equiv |\langle \Psi(T) | \Psi_{\text{MES}} \rangle|^2, \tag{33}$$

which defines the expectation value of the projection operator $|\Psi_{\text{MES}}\rangle\langle\Psi_{\text{MES}}|$, where $|\Psi_{\text{MES}}\rangle \equiv \sqrt{\frac{1}{2M+1}} \sum_{m=-M}^{M} |m\rangle \otimes |m\rangle$ is a maximally entangled state (for a basis set truncated at M) [37]. Maximization of the cost function in Eq. (33) also maximizes the von Neumann entropy S_{vN} [50,51], such that $S_{vN}(|\Psi_{\text{MES}}\rangle) = \ln(2M+1)$.

2. Three-rotor objectives

The following two control objectives are considered for the three-rotor system described in Sec. V A 3.

(i) Identical orientation of the three rotors, where the objective functional is

$$J_{id}^{[3]}(T) \equiv \langle \cos\phi_1 + \cos\phi_2 + \cos\phi_3 \rangle(T), \tag{34}$$

which seeks orientation of all three rotors in the $+\hat{\mathbf{x}}$ direction.

(ii) Opposing orientations of the three-rotor system, where the objective functional is

$$J_{\text{opp}}^{[3]}(T) = \langle -\cos\phi_1 + \cos\phi_2 \rangle(T), \tag{35}$$

which is equivalent to $J_{\text{opp}}^{[3]}(T) = \langle -\cos\phi_3 + \cos\phi_2 \rangle(T)$ [cf. Eq. (31)]. Maximization of this objective corresponds to orienting rotor 2 in the $+\hat{\mathbf{x}}$ direction, and orienting rotors 1 and 3 in the $-\hat{\mathbf{x}}$ direction.

VI. EFFECT OF SEPARATION ON THE FIRST-ORDER MAGNUS EXPANSION

This section numerically investigates the effect of perturbation strength on approximation quality. Specifically, benchmark simulations were performed to examine how the rotor separation affects the accuracy of the first-order Magnus expansion, for the two- and three-rotor systems described in Sec. V A. Note that the simulations here are concerned with the accuracy of the approximate time evolution itself and do not involve any optimization. For comparison, simulations were also performed to evaluate the accuracy of the zeroth-order approximation [i.e., evolution under the tensor product expression in Eq. (20) implemented using small time step operators].

Five different fields were randomly generated of the form

$$\varepsilon_{\text{rand}}(t) = \alpha_0 \sum_{m=0}^{3} \beta_m \cos(\omega_m t + \delta_m), \tag{36}$$

where β_m and δ_m are random numbers generated between (0,1) and (0,2π), respectively, $\alpha_0 = 5 \times 10^6 \frac{N}{C}$, and $\omega_m = \frac{B(2m+1)}{\hbar}$ is the field-free, coupling-free, individual rotor transition frequency from $|m\rangle$ to $|m+1\rangle$. For both two rotors and three rotors, a collection of rotor separations between $R = 4$ nm and $R = 8$ nm were considered. For each of these systems, simulations were performed using each of the five random fields from Eq. (36) in order to compute the approximate final states under the zeroth-order model ($|\Psi^{(0)}(T)\rangle$) and first-order Magnus expansion ($|\Psi_{M1}(T)\rangle$), as well as the reference final state ($|\Psi_{\text{ref}}(T)\rangle$) under the exact simulation. For these simulations, $T = 1.306$ ns, $M = 4$, and $n = 999$ were used. In each case, the overlaps $|\langle \Psi_{M1}(T) | \Psi_{\text{ref}}(T) \rangle|$ and $|\langle \Psi^{(0)}(T) | \Psi_{\text{ref}}(T) \rangle|$ were computed as metrics of approximation accuracy.

The aggregated results are plotted in Fig. 2. These plots show that the first-order Magnus expansion clearly improves upon the accuracy of the zeroth-order approximation at all separations, and that both approximations are more accurate at larger separations (this is as expected since the dipole-dipole coupling strength scales as $\frac{1}{R^3}$). For the largest separations considered here, the difference in accuracy between the first-order Magnus expansion and the zeroth-order approximation (which completely neglects the couplings between rotors) becomes relatively minimal. Therefore, the first-order Magnus expansion is likely most practically useful in the intermediate regime where it has a reasonably high accuracy, while also still provides a significant improvement over the zeroth-order approximation. Additionally, for each separation R, the accuracy of the first-order Magnus expansion has a smaller statistical variation than that of the zeroth-order approximation.

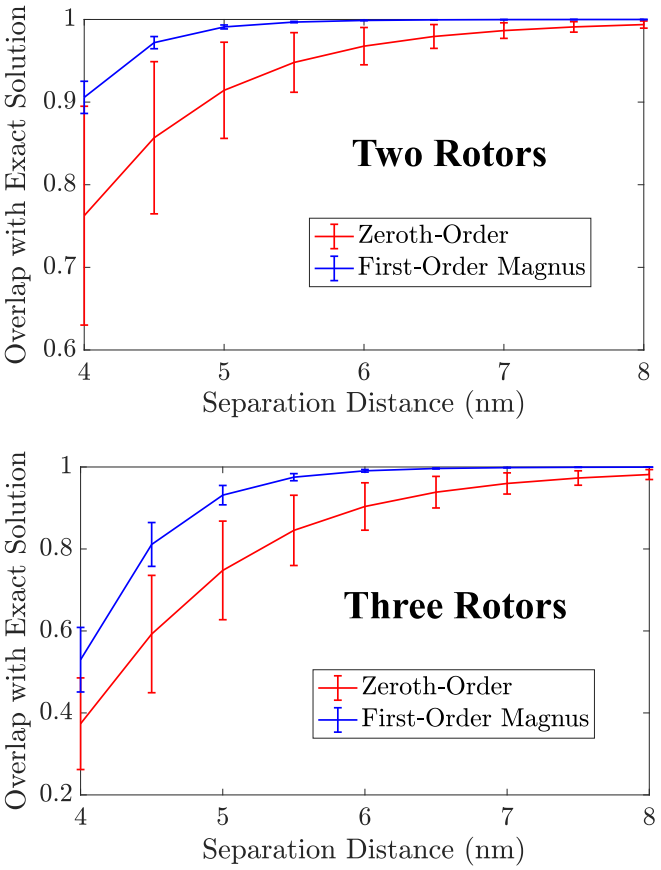

FIG. 2. Aggregated results for approximation accuracy versus rotor separation from the benchmark simulations. In both plots, the blue curve corresponds to the overlap between the final states of the first-order Magnus and exact simulations, $|\langle\Psi_{M1}(T)|\Psi_{\text{ref}}(T)\rangle|$; the red curve corresponds to the overlap between the final states of the zeroth-order and exact simulations, $|\langle\Psi^{(0)}(T)|\Psi_{\text{ref}}(T)\rangle|$. Each point on the curves represents an average value taken over the five randomly generated fields in Eq. (36), and the error bars represent one standard deviation. The top plot shows the results for two rotors, and the bottom plot shows the results for three rotors.

VII. OPTIMAL CONTROL NUMERICAL SIMULATIONS

This section presents optimal control simulations for the two-rotor and three-rotor control objectives described in Sec. V B. For all simulations, the initial trial field $\varepsilon_{\text{trial}}(t)$ is taken to have a Gaussian envelope along with F characteristic frequencies of the system, i.e.,

$$\varepsilon_{\text{trial}}(t) = a_0 \exp\left(-\frac{\left(t-\frac{T}{2}\right)^2}{\left(\frac{T}{2\sqrt{7}}\right)^2}\right)\sum_{m=0}^{F-1} b_m \cos(\omega_m t), \qquad (37)$$

where a_0 and $\{b_m\}$ are constants selected for the particular simulation ($\omega_m = \frac{B(2m+1)}{\hbar}$ is the same as defined in Sec. VI). This initial trial field was then optimized in subsequent iterations with the stochastic hill climbing algorithm. Note that Eq. (37) serves only as the form of the initial trial field, and not as a constraint on the form that the field can take during optimization [i.e., the optimized field is not required to have the Gaussian envelope and F characteristic frequencies of Eq. (37)]. For each example, the choices of rotor separation R and final time T were guided by the benchmark simulations of accuracy vs separation presented in Sec. VI, as well as the results in [12] and [37].

To evaluate the approximation accuracy in each case, the exact simulation [cf. Eq. (5)] is performed using the optimal field that was determined within the first-order Magnus expansion. Note that this type of practice for assessing the accuracy of approximate quantum optimal control was also employed in, for example, [52]. Additionally, to characterize the control field strength, the ratio $\frac{\mu|\varepsilon|_{\max}}{B}$ was computed after the optimization was completed, where $|\varepsilon|_{\max}$ is the maximum magnitude of the optimal field $\varepsilon(t)$. The ratio is a measure of the strength of the local potential due to the control field relative to the lowest field-free, coupling-free, individual rotor energy level spacing (between states $|0\rangle$ and $|1\rangle$), cf. Sec. V A 1. For the four numerical examples in this section, the value of $\frac{\mu|\varepsilon|_{\max}}{B}$ ranged between 3.85 and 4.91, indicating that all of the illustrations were in the strong control field regime.

The simulation results for each of the four control objectives are summarized in Table I and discussed in Secs. VII A and VII B. Note that for each orientation case, the theoretical maximum value of $\langle\cos\phi_i\rangle$ is given by the largest eigenvalue of the operator $\cos\phi_i$ in the corresponding truncated basis set [37]. Section S6 provides additional details on the numerical approach and results, including numerical evidence of convergence with respect to M [42].

A. Two-rotor optimal control simulations

1. Orientation

The optimal control simulation of the two-rotor orientation objective (see Sec. V B 1) is performed with $R = 5$ nm, $T = 1.306$ ns, and $M = 8$. The optimal field $\varepsilon(t)$ yielded $\langle\cos\phi_1\rangle(T) = \langle\cos\phi_2\rangle(T) = 0.980$ in the first-order Magnus expansion. Using this optimal field in the exact simulation produced $\langle\cos\phi_1\rangle(T) = \langle\cos\phi_2\rangle(T) = 0.970$ (see Table I). Hence, a high value of $J_{or}^{[2]}$ was achieved, and importantly, very little drop-off in objective occurs when using the optimal field determined within the first-order Magnus expansion in the exact simulation. The theoretical maximum value of $\langle\cos\phi_i\rangle$ in this basis set is 0.985.

2. Entanglement

The optimal control simulation of the two-rotor entanglement objective (see Sec. V B 1) utilized $T = 3.921$ ns, $R = 7$ nm, and $M = 4$. The optimal field $\varepsilon(t)$ yielded an objective value of $J_{\text{ent}}^{[2]} = 0.956$ in the first-order Magnus expansion, compared to a value of $J_{\text{ent}}^{[2]} = 0.825$ for the same field in the exact simulation (see Table I). The von Neumann entropies of the final states were $S_{vN} = 2.113$ within the first-order Magnus expansion and $S_{vN} = 2.021$ for the same field in the exact simulation. Both values are close to the theoretical maximum possible entropy $S_{vN}(|\Psi_{\text{MES}}\rangle) = 2.197$ in the $M = 4$ basis (see Sec. V B 1). This substantial degree of entanglement is important because it was achieved despite starting from a zero entropy initial state and treating dipolar coupling only as a perturbation (note that entropy is always zero in the zeroth-order approximation).

TABLE I. Collective results of the optimal control simulations. The first column lists the control objective for each simulation. The second column shows the objective values obtained utilizing the first-order Magnus expansion. The third column shows the values obtained from performing an exact simulation using the optimal field determined from the first-order Magnus expansion. Here the notation $\langle\cos\phi_{i,j}\rangle \equiv \langle\cos\phi_i\rangle = \langle\cos\phi_j\rangle$ is used when $\langle\cos\phi_i\rangle = \langle\cos\phi_j\rangle$ is guaranteed by symmetry.

Optimal control objective	First-order Magnus expansion	Exact simulation
Two-rotor orientation	$\langle\cos\phi_{1,2}\rangle(T) = 0.980$	$\langle\cos\phi_{1,2}\rangle(T) = 0.970$
Two-rotor entanglement	$\lvert\langle\Psi(T)\rvert\Psi_{\mathrm{MES}}\rangle\rvert^2 = 0.956$	$\lvert\langle\Psi(T)\rvert\Psi_{\mathrm{MES}}\rangle\rvert^2 = 0.825$
Three-rotor identical orientations	$\langle\cos\phi_{1,3}\rangle(T) = 0.958$ $\langle\cos\phi_2\rangle(T) = 0.958$	$\langle\cos\phi_{1,3}\rangle(T) = 0.952$ $\langle\cos\phi_2\rangle(T) = 0.952$
Three-rotor opposing orientations	$\langle\cos\phi_{1,3}\rangle(T) = -0.735$ $\langle\cos\phi_2\rangle(T) = 0.878$	$\langle\cos\phi_{1,3}\rangle(T) = -0.589$ $\langle\cos\phi_2\rangle(T) = 0.626$

B. Three-rotor optimal control simulations

1. Identical orientations

The optimal control simulation of the three-rotor identical orientations objective (see Sec. V B 2) employed $R = 6.29$ nm, $T = 1.306$ ns, and $M = 5$. The optimal field $\varepsilon(t)$ for the three-rotor system yielded $\langle\cos\phi_1\rangle(T) = \langle\cos\phi_3\rangle(T) = 0.958$ and $\langle\cos\phi_2\rangle(T) = 0.958$, in the first-order Magnus expansion. In comparison, the values $\langle\cos\phi_1\rangle(T) = \langle\cos\phi_3\rangle(T) = 0.952$ and $\langle\cos\phi_2\rangle(T) = 0.952$ were computed using the same control field within the exact simulation (see Table I). This result shows achievement of a high value of $J_{id}^{[3]}$ with very little difference in value between the first-order Magnus and exact simulations. The theoretical maximum value of $\langle\cos\phi_i\rangle$ in this basis set is 0.966.

2. Opposing orientations

The optimal control simulation of the three-rotor opposing orientations objective (see Sec. V B 2) utilized $R = 8.5$ nm, $T = 3.921$ ns, and $M = 5$. The optimal field $\varepsilon(t)$ yielded the final orientations $\langle\cos\phi_1\rangle(T) = \langle\cos\phi_3\rangle(T) = -0.735$ and $\langle\cos\phi_2\rangle(T) = 0.878$, within the first-order Magnus expansion. Using the same optimal field, the orientations $\langle\cos\phi_1\rangle(T) = \langle\cos\phi_3\rangle(T) = -0.589$ and $\langle\cos\phi_2\rangle(T) = 0.626$ were computed for the exact simulation (see Table I). The drop-off in objective when using the Magnus-determined optimal field within the exact simulation is relatively modest, considering that in the zeroth-order approximation orientations are always identical. Since this simulation used the same basis set as the one in Sec. VII B 1, the theoretical maximum value of $\langle\cos\phi_i\rangle$ was again given by 0.966.

VIII. CONCLUSIONS

This paper presented a practical approach for performing approximate optimal control simulations of quantum systems with multiple coupled degrees of freedom. The first-order Magnus expansion in the interaction picture is utilized, treating the couplings between different degrees of freedom as the perturbation. The inclusion of the control field in the zeroth-order Hamiltonian allows for good accuracy in the strong field regime. The Magnus expansion formulation can readily be combined with gradient-free approaches to control field optimization, such as the stochastic hill climbing algorithm adopted in this paper. To give a sense of the cost savings possible for the case of pairwise couplings, it was shown that in the large N limit the cost per iteration with the first-order Magnus expansion is reduced by a factor of n versus that of the exact simulation. This saving arises (i) from the ability to skip the computation of the state at intermediate times together with (ii) the ready computation of $\Omega_{I,1}(T)$ enabled by pairwise couplings and the separability of the zeroth-order time evolution operator.

The four optimal control numerical illustrations, all of which were in the strong field regime, highlight that the approach can be used to optimize control fields to drive systems of rotors to a range of different objectives. In particular, the two-rotor system provided examples of optimal control of orientation and of entanglement, and the three-rotor system demonstrated optimal control of identical and opposing orientations. The entanglement and opposing orientation objectives are particularly interesting because they are not achievable to any extent in the zeroth-order approximation, so inclusion of the dipole-dipole coupling term is essential. Moreover, the ability to generate entanglement is of central importance for quantum information applications [14,15,50,51].

Further quantum optimal control studies using a Magnus-based approach could consider different physical systems and objectives as well as other optimization algorithms. Additional research could also investigate various means for reducing the computational cost, such as using more efficient numerical methods, exploiting physical symmetries, or approximating the final exponentiation required for the first-order Magnus expansion. Future work could also investigate whether the field obtained from the approximate optimal control method makes for a good trial field for the exact optimization problem. Finally, we hope this work can motivate the development of new methods for many-body quantum optimal control theory, which is a challenging area of research.

ACKNOWLEDGMENTS

We thank Nicolas Boumal, Nicholas Higham, and Adam Marcus for helpful discussions on numerical methods and computational scaling. A.B.M. acknowledges support from the DOE CSGF Grant No. DE-FG02-97ER25308. T.S.H. acknowledges support from DOE Grant No. DE-FG02-02ER15344, and H.R. from ARO Grant No. W911NF-16-1-0014.

[1] C. Brif, R. Chakrabarti, and H. Rabitz, New J. Phys. **12**, 075008 (2010).

[2] R. Kosloff, S. A. Rice, P. Gaspard, S. Tersigni, and D. J. Tannor, Chem. Phys. **139**, 201 (1989).

[3] A. P. Peirce, M. A. Dahleh, and H. Rabitz, Phys. Rev. A **37**, 4950 (1988).

[4] S. Shi, A. Woody, and H. Rabitz, J. Chem. Phys. **88**, 6870 (1988).

[5] J. Werschnik and E. K. U. Gross, J. Phys. B **40**, R175 (2007).

[6] N. Khaneja, T. Reiss, C. Kehlet, T. Schulte-Herbrüggen, and S. J. Glaser, J. Magn. Reson. **172**, 296 (2005).

[7] Y. Maday and G. Turinici, J. Chem. Phys. **118**, 8191 (2003).

[8] A. Rothman, T. S. Ho, and H. Rabitz, J. Chem. Phys. **123**, 134104 (2005).

[9] W. Zhu and H. Rabitz, J. Chem. Phys. **109**, 385 (1998).

[10] T. Caneva, T. Calarco, and S. Montangero, Phys. Rev. A **84**, 022326 (2011).

[11] K. Krieger, A. Castro, and E. K. U. Gross, Chem. Phys. **391**, 50 (2011).

[12] A. Magann, L. Chen, T. S. Ho, and H. Rabitz, J. Chem. Phys. **150**, 164303 (2019).

[13] C. Arenz and H. Rabitz, Phys. Rev. Lett. **120**, 220503 (2018).

[14] F. Dolde, V. Bergholm, Y. Wang, I. Jakobi, B. Naydenov, S. Pezzagna, J. Meijer, F. Jelezko, P. Neumann, T. Schulte-Herbrüggen, J. Biamonte, and J. B. Wrachtrup, Nat. Comm. **5**, 3371 (2014).

[15] G. Waldherr, Y. Wang, S. Zaiser, M. Jamali, T. Schulte-Herbrüggen, H. Abe, T. Ohshima, J. Isoya, J. F. Du, P. Neumann, and J. Wrachtup, Nature (London) **506**, 204 (2014).

[16] D. J. Tannor and S. A. Rice, J. Chem. Phys. **83**, 5013 (1985).

[17] I. Grigorenko and H. Rabitz, Appl. Phys. Lett. **94**, 253107 (2009).

[18] C. Winterfeldt, C. Spielmann, and G. Gerber, Rev. Mod. Phys. **80**, 117 (2008).

[19] T. Caneva, A. Silva, R. Fazio, S. Lloyd, T. Calarco, and S. Montangero, Phys. Rev. A **89**, 042322 (2014).

[20] P. Doria, T. Calarco, and S. Montangero, Phys. Rev. Lett. **106**, 190501 (2011).

[21] B. Kohler, J. L. Krause, R. Raksi, C. Rose-Petruck, R. M. Whitnell, K. R. Wilson, V. Yakovlev, and Y. Yan, *Reaction Dynamics in Clusters and Condensed Phases* (Springer, Berlin/Heidelberg, 1993).

[22] M. Messina and K. R. Wilson, Chem. Phys. Lett. **241**, 502 (1995).

[23] C. S. Guiang and R. E. Wyatt, J. Chem. Phys. **112**, 3580 (2000).

[24] M. Messina, K. R. Wilson, and J. L. Krause, J. Chem. Phys. **104**, 173 (1996).

[25] M. Schröder and A. Brown, J. Chem. Phys. **131**, 034101 (2009).

[26] M. Schröder, J. L. Carreón-Macedo, and A. Brown, Phys. Chem. Chem. Phys. **10**, 850 (2008).

[27] L. Wang, H. D. Meyer, and V. May, J. Chem. Phys. **125**, 014102 (2006).

[28] S. Blanes, F. Casas, J. A. Oteo, and J. Ros, Phys. Rep. **470**, 151 (2009).

[29] N. E. Henriksen, Chem. Phys. Lett. **312**, 196 (1999).

[30] M. S. Child, *Molecular Collision Theory* (Academic Press, Cambridge, 1974).

[31] A. Rosete-Suárez, A. Ochoa-Rodríguez, and M. Sebag, in *Proceedings of the 1st Annual Conference on Genetic and Evolutionary Computation – Volume 2* (Morgan Kaufmann Publishers Inc., 1999), pp. 1699–1706.

[32] J. Salomon, C. M. Dion, and G. Turinici, J. Chem. Phys. **123**, 144310 (2005).

[33] G. Turinici and H. Rabitz, J. Phys. A **43**, 105303 (2010).

[34] M. Yoshida and Y. Ohtsuki, Chem. Phys. Lett. **633**, 169 (2015).

[35] A. Magann, T. S. Ho, and H. Rabitz, Phys. Rev. A **98**, 043429 (2018).

[36] K. Mishima and K. Yamashita, J. Chem. Phys. **130**, 034108 (2009).

[37] H. Yu, T. S. Ho, and H. Rabitz, Phys. Chem. Chem. Phys. **20**, 13008 (2018).

[38] J. Zhu, S. Kais, Q. Wei, D. Herschbach, and B. Friedrich, J. Chem. Phys. **138**, 024104 (2013).

[39] Y. Ohtsuki and T. Namba, J. Chem. Phys. **151**, 164107 (2019).

[40] B. P. Abolins, R. E. Zillich, and K. B. Whaley, J. Chem. Phys. **148**, 102338 (2018).

[41] Y. Y. Liao, S. R. Jian, and J. R. Lee, Eur. Phys. J. D **73**, 47 (2019).

[42] See Supplemental Material at http://link.aps.org/supplemental/10.1103/PhysRevA.102.013115 for mathematical formulations for second-order and multistep Magnus expansions, implementation and computational cost details for the first-order Magnus expansion, a suggested implementation and computational cost analysis for the second-order Magnus expansion, details on the stochastic hill climbing algorithm, a proof of relevant physical symmetries in the three-rotor system, and details on the optimal control numerical illustrations. Also, see Refs. [55–58].

[43] R. Kosloff, J. Phys. Chem. **92**, 2087 (1988).

[44] More precisely, it requires computing the product of a matrix exponential and a vector ($e^A v$). See, e.g., [53] and [54] and the discussion in Sec. S2 [42].

[45] M. Demiralp and H. Rabitz, Phys. Rev. A **47**, 809 (1993).

[46] This can be seen as follows. From Eqs. (10) and (17), $H_I^{(1)}(t) = U^{(0)}(t)^\dagger W U^{(0)}(t)$. Therefore, for any unitary-invariant matrix norm (e.g., the standard spectral norm used in [28] for characterizing the Magnus expansion), $||H_I^{(1)}(t)|| = ||W||$, which is independent of the control field $\varepsilon(t)$.

[47] C. Moler and C. V. Loan, SIAM Rev. **45**, 3 (2006).

[48] A. G. Maki, J. Phys. Chem. Ref. Data **3**, 221 (1974).

[49] R. G. Shulman and C. H. Townes, Phys. Rev. **77**, 500 (1950).

[50] L. Amico, R. Fazio, A. Osterloh, and V. Vedral, Rev. Mod. Phys. **80**, 517 (2008).

[51] M. A. Nielsen and I. L. Chuang, *Quantum Computation and Quantum Information* (Cambridge University Press, Cambridge, 2000).

[52] M. Keck, M. M. Müller, T. Calarco, and S. Montangero, Phys. Rev. A **92**, 033402 (2015).

[53] A. H. Al-Mohy and N. J. Higham, SIAM J. Sci. Comput. **33**, 488 (2011).

[54] N. J. Higham and A. H. Al-Mohy, Acta Numer. **19**, 159 (2010).

[55] F. Le Gall, in *Proceedings of the 39th International Symposium on Symbolic and Algebraic Computation* (Association for Computing Machinery, New York, 2014).

[56] J. R. Gilbert, SIAM J. Matrix Anal. Appl. **15**, 62 (1994).

[57] C. Lanczos, J. Res. Natl. Bur. Stand. **45**, 255 (1950).

[58] R. B. Sidje and W. J. Stewart, Comput. Stat. Data Anal. **29**, 345 (1999).